Integrated Sensors of Rotor Position and Speed Based on Signal Injection for IPM–Synchronous Motor Drives

Gheorghe Daniel Andreescu
Dept. of Automation and Industrial Informatics
University "Politehnica" of Timisoara
Blvd. Vasile Parvan 2, 300223 Timisoara
Romania
dandre@aut.utt.ro

Ion Boldea
Dept. of Electrical Engineering and Drives
University "Politehnica" of Timisoara
Blvd. Vasile Parvan 2, 300223 Timisoara
Romania
boldea@lselinux.utt.ro

Abstract – **The paper comparatively studies and develops on three integrated sensors (estimators) of rotor position and speed based on rotating carrier-voltage injection for sensorless control of IPM-synchronous motor drives. These estimators operate in different reference frames and basically contain: i) a band-pass filter (BPF) to extract a specific carrier-current harmonic generated by the magnetic saliency, and ii) a phase-locked loop tracking observer to extract the rotor position contained in the phase of selected harmonic. The harmonics have a small level in high inverter-switching noise. A novel estimator in stator reference, with lower computation effort, which employs for BPF a recent efficient vector filter in D-module with frequency sign selectivity, is proposed. The estimations are thus made insensitive to motor parameters and noise. Extensive digital simulation results prove the effectiveness and the equivalence of the three estimators at low speed including zero speed.**

I. INTRODUCTION

The interior permanent magnet synchronous motor (IPMSM) is extensively used in high-performance applications due to its high efficiency and wide constant power speed range [1]. The IPMSM drives require rotor position and speed for vector and motion control. Rotor shaft sensors add supplementary cost, volume and weight and reduce reliability. Therefore, the integrated sensors for sensorless control are developed using only stator current and eventually voltage measurements.

Sensorless control methods are mainly divided into two categories [2]: 1) electromotive force (emf) tracking based on fundamental model that fail at zero and low speed, and 2) saliency tracking based on signal injection suitable for low speed operation, including zero speed.

The signal injection methods exploit the magnetic anisotropies that contain the rotor position information. The IPMSM saliency is given by a large intrinsic spatial-saliency due to high inductance ratio L_q/L_d = 2–4, and a small saturation-induced saliency. The injected test signals can be: a) persistent high-frequency (hf) voltage [2-9], b) discrete voltage pulses [10], c) modified PWM pulses [2].

Fig. 1 shows the principle of the saliency tracking methods using rotating hf voltage injection in IPMSM sensorless control. Basically, a small rotating carrier-voltage with higher frequency $\underline{u}_c = V_c \exp(j\omega_c t)$, $V_c < 10$V, ω_c = 300–1000 Hz, is injected superimposing on top of driving fundamental stator-voltage $\underline{u}_s$. The resulting carrier-current $\underline{i}_c$, modulated by the position dependent inductances, contains rotor position information θ_r. A low-pass filter (LPF) selects the fundamental current $\underline{i}_s$ used in vector control. A band-pass filter (BPF) in a specific reference selects an explicit carrier-current harmonic $\underline{i}_{cx}$.

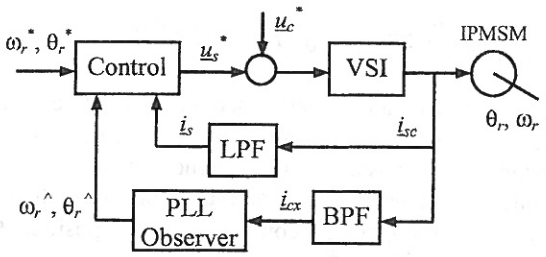

Fig. 1. Principle of sensorless control using rotating hf voltage injection

BPF is cascaded by a phase-locked loop (PLL) tracking observer that extracts the rotor position and speed estimations. The spatial-saliency tracking methods are independent of model parameters and speed (emf).

This paper focuses to study and build on three integrated sensors (estimators) of rotor position and speed based on signal injection and spatial-saliency for sensorless control of IPMSM. They are: 1) the saliency-tracking estimator in carrier reference [3-6], 2) the mirror-phase estimator in estimated rotor reference [8], 3) new saliency-tracking estimator with vector filter in D-module in stator reference. Extensive digital simulation results demonstrate the effectiveness and the equivalence of these integrated sensors at low and zero speed.

II. IPMSM MODEL INCLUDING SATURATION FOR CARRIER SIGNAL INJECTION

The IPMSM voltage model in stator reference [1, 5] is given in vector form by

$$\underline{u}_s = R_s \underline{i}_s + \frac{d}{dt}(\Sigma L \underline{i}_s + \Delta L\, e^{j2\theta_r} \underline{i}_s^*) + j\omega_r \lambda_M e^{j\theta_r}, \quad \text{with } \Sigma L = (L_d + L_q)/2 \text{ and } \Delta L = (L_d - L_q)/2, \tag{1}$$

where: $\underline{u}_s$, $\underline{i}_s$ are the stator voltage and current vectors, R_s is the stator resistance, $L_d(i_s)$, $L_q(i_s)$ are the d, q inductances depending on i_s magnitude due to magnetic saturation, λ_M is the PM flux, θ_r, ω_r are the rotor position and speed, and the symbol * refers to conjugate operator.

The rotating hf carrier-voltage injection $\underline{u}_c$ is added to the fundamental driving voltage-vector in stator reference.

$$\underline{u}_c = V_c e^{j\theta_c}, \quad \theta_c = \omega_c t. \tag{2}$$

The injected carrier-voltage excites the machine at higher frequency than the fundamental and interacts with the saliency (intrinsic by spatial and induced by saturation)

Remark: The hf carrier-voltage effect generates stator carrier-current harmonics $\underline{i}_c$ containing information on the rotor position. The carrier-current is superimposed to the

fundamental stator current with an *independent behavior*.

Neglecting the resistance voltage drop, and the rotation induced voltage for $\omega_r << \omega_c$, the stator carrier-current $\underline{i}_c$ is obtained from (1) with $\underline{u}_s = \underline{u}_c$. The d-axis current is approximated with respect to the d-axis flux linkage by a 2nd order Taylor expansion, neglecting the cross-saturation terms [4-5]. Finally, the stator-current $\underline{i}_{sc}$ contains the fundamental $\underline{i}_s$ and carrier-harmonic terms $\underline{i}_c$ [4]:

$$\underline{i}_{sc} = I_s e^{j(\theta_r+\Phi_s)} + I_{cp1} e^{j(\theta_c-\pi/2)} + I_{cn1} e^{j(-\theta_c+2\theta_r+\pi/2)} + I_{cp2} e^{j(2\theta_c-\theta_r-\Phi_{p2})} + I_{cn2} e^{j(-2\theta_c+3\theta_r+\Phi_{n2})}, \quad (3)$$

with $I_{cp1} \approx \dfrac{V_c \Sigma L}{\omega_c L_d L_q}$, and $I_{cn1} \approx \dfrac{V_c \Delta L}{\omega_c L_d L_q}$.

There are positive and negative sequences relative to the injected carrier-frequency ω_c. The 1st harmonics are generated by intrinsic spatial saliency, while the 2nd harmonics are generated by saturation-induced saliency. The sequence components contain the rotor position θ_r, except for the positive (1st) sequence.

Fig. 2 shows an example of carrier-current spectrum for $\omega_r << \omega_c$ [4] associated to (3). The negative sequence has high amplitude comparing to the 2nd positive and negative sequences that are very small.

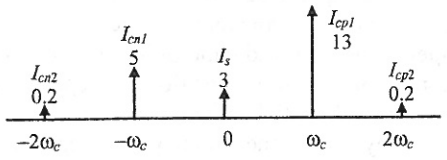

Fig. 2. Carrier-current spectrum in stator reference for $\omega_r << \omega_c$

III. ESTIMATORS BASED ON SIGNAL INJECTION

A. Saliency Tracking Estimator in Carrier Reference

Fig. 3 shows the spatial-saliency tracking estimator in carrier reference (STe-Cr) developed from [3-4].

The carrier-current harmonic terms in carrier reference $\underline{i}^c_c = \underline{i}_c \exp(j\theta_c)$, where $\theta_c = \omega_c t$, have the following central phases: θ_c, $2\theta_c$, $2\theta_r$, $3\theta_c$, $-\theta_c$. The negative sequence in carrier reference $\underline{i}^c_{cn1} = I_{cn1} \exp\{j(2\theta_r + \pi/2)\}$ is selected by the low-pass filter (LPF). The PLL observer extracts the phase of this harmonic, i.e., rotor position estimation $\hat{\theta}_r$.

The PLL error $\varepsilon \sim \Delta\theta_r = \theta_r - \hat{\theta}_r$ is obtained using a unit vector from the vector-product imaginary part:

$$\varepsilon = Im\,[\underline{i}^c_{cn1} \exp\{-j(2\hat{\theta}_r + \pi/2)\}] \cong 2 I_{cn1} \Delta\theta_r. \quad (4)$$

The PLL employs a simple state filter estimator

$$\begin{bmatrix} \hat{\theta}_r \\ \hat{\omega}_r \end{bmatrix}^{\bullet} = \begin{bmatrix} 0 & 1 \\ 0 & 0 \end{bmatrix} \begin{bmatrix} \hat{\theta}_r \\ \hat{\omega}_r \end{bmatrix} + \begin{bmatrix} k_p \\ k_i \end{bmatrix} \Delta\theta_r, \quad \begin{bmatrix} \hat{\theta}_r \\ \hat{\omega}_r \end{bmatrix}_{t=0} = \begin{bmatrix} \hat{\theta}_{r0} \\ \hat{\omega}_{r0} \end{bmatrix}, \quad (5)$$

where $[k_p, k_i]^T$ is the correction matrix and $\hat{\theta}_r$ is modulo 2π.

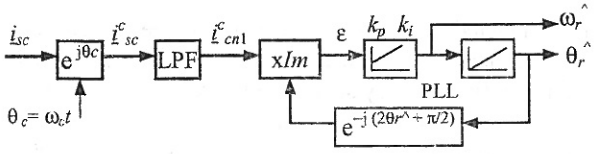

Fig.3. Spatial-saliency tracking estimator in carrier reference (STe-Cr)

To improve dynamic estimations of the rotor position and speed, an extended Luenberger observer (6) with zero-phase lag [2-5] (Fig. 4) can be used. It is based on the full mechanical model having as main input the estimated electromagnetic torque T_e (7), or the reference torque T_e^* given by the motion controller. The observer intrinsically offers also the disturbance torque T_L as extended state variable that can be used to disturbance rejection in motion control to improve the robustness to the load torque.

$$\begin{bmatrix} \hat{\theta}_r \\ J\hat{\omega}_r \\ \hat{T}_L \end{bmatrix}^{\bullet} = \begin{bmatrix} 0 & 1 & 0 \\ 0 & 0 & -1 \\ 0 & 0 & 0 \end{bmatrix} \begin{bmatrix} \hat{\theta}_r \\ \hat{\omega}_r \\ \hat{T}_L \end{bmatrix} + \begin{bmatrix} 0 \\ 1 \\ 0 \end{bmatrix} \hat{T}_e + \begin{bmatrix} k_1 \\ k_2 \\ k_3 \end{bmatrix} \Delta\theta_r. \quad (6)$$

$$\hat{T}_e = 3/2\, p\,[\lambda_M \hat{i}_q + (L_d - L_q)\hat{i}_d \hat{i}_q], \quad (7)$$

where p is the number of pole pairs, $\hat{J}$ is the equivalent rotor inertia, $\hat{i}_d$, $\hat{i}_q$ are the stator-current components in estimated rotor reference $\hat{\theta}_r$. The matrix $[k_1\ k_2\ k_3]^T$ for state correction is designed using the pole allocation method, e.g., tuned for a 100 Hz bandwidth [3].

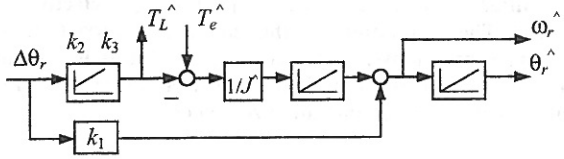

Fig. 4. Zero-phase lag extended Luenberger observer

B. Mirror-Phase Estimator in Estimated Rotor Reference

Fig. 5 shows the mirror-phase based estimator in estimated rotor reference (MPe-Rr).

The negative and positive sequence of the carrier-current in estimated rotor reference $\underline{i}^r_c = \underline{i}_c \exp(-j\hat{\theta}_r)$ are:

$$\underline{i}^r_{cn1} = I_{cn1} \exp\{j(-\theta_c + 2\theta_r - \hat{\theta}_r + \pi/2)\},$$
$$\underline{i}^r_{cp1} = I_{cp1} \exp\{j(\theta_c - \hat{\theta}_r - \pi/2)\}. \quad (8)$$

The PLL error $\varepsilon \sim \Delta\theta_r$ is obtained from the vector-product imaginary part:

$$\varepsilon = Im\,[\underline{i}^r_{cn1}\, \underline{i}^r_{cp1}] \cong 2 I_{cn1} I_{cp1} \Delta\theta_r. \quad (9)$$

PLL error (9) is a simple and natural solution comparing with other three different solutions proposed in [8].

The carrier-current components $\underline{i}^r_{cn1}$ and $\underline{i}^r_{cp1}$ (8) have the same frequency magnitude ω_c, but opposite frequency sign. They are extracted separately from the stator current using recent vector (two-input/output) filters in D-module having both frequency and sign selectivity properties [9].

This approach leads to the same structure as the mirror-phase based approach [8], but in a more straightforward and simple way.

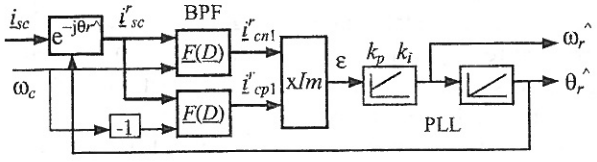

Fig. 5. Mirror-phase estimator in estimated rotor reference (MPe-Rr)

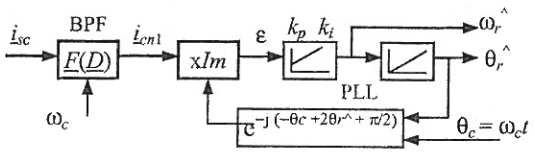

Fig. 6. New estimator with filter in D-module in stator ref. (FDe-Sr)

C. New Estimator with Filter in D-Module in Stator Reference

The new proposed estimator with filter in D-module in stator reference (FDe-Sr) is shown in Fig. 6.

The carrier-current negative sequence in stator reference $\underline{i}_{cn1} = I_{cn1} \exp\{j(-\theta_c + 2\theta_r + \pi/2)\}$ is selected by the vector BPF using the filter in D-module with the centre frequency ω_c. The PLL observer extracts the rotor position and speed estimations using the PLL error $\varepsilon \sim \Delta\theta_r$ obtained from the vector-product imaginary part:

$$\varepsilon = Im\,[\underline{i}_{cn1} \exp\{-j(-\theta_c + 2\theta_r^\wedge + \pi/2)\}] \cong 2I_{cn1}\,\Delta\theta_r. \qquad (10)$$

The new solution preserves the advantages of the BPF based on filter in D-module. Moreover, it has a simpler implementation comparing with mirror-phase estimator.

1) Vector (Two-Input/Output) Filter in D-Module: This class of vector filters discriminates the phase-polarity, which is essential to solve the problems bellow. Moreover, they are insensitive to motor parameters.

Let be a n^{th}-order scalar filter, e.g., for simplicity $n = 2$, which has the transfer function

$$F(s) = \frac{b_2 s^2 + b_1 s + b_0}{s^2 + a_1 s + a_0}. \qquad (11)$$

The associated vector filter in D-module $\underline{F(D)}$ [8-9], with the filtering property $\underline{F}(s + j\omega_c)$, has the realization in vector D-module direct form I presented in Fig. 7a. The realization of inverse $\underline{D}^{-1}$ module is shown in Fig. 7b.

2) The Design of Filter in D-Module is based on the following main property [8]: if the scalar (single-input/output) filter $F(s)$ (11) is designed as a low-pass filter (LPF) with the bandwidth B, then the associated vector (two-input/output) filter in D-module $\underline{F}(\underline{D}(s, -\omega_c))$ is a band-pass filter (BPF) with the centre frequency ω_c, having the same bandwidth B.

Remarks: The structure of the inverse $\underline{D}^{-1}$ module (Fig. 7b) rejects dc-offset and drifts from the stator-current acquisition chains.

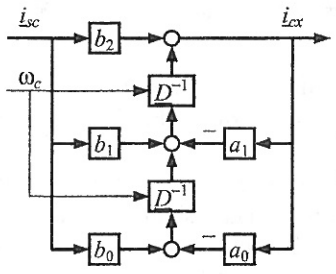

Fig. 7a.

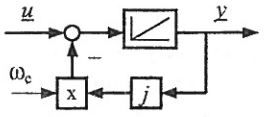

Fig. 7b.

Fig. 7. a.) 2^{nd} order vector filter $\underline{F}(\underline{D}(s, \omega_c))$ in D-module direct form I
b.) Realization of inverse $\underline{D}^{-1}(s, \omega_c)$ module

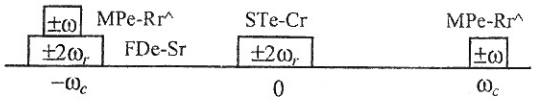

Fig. 8. BPF frequency distribution of signal injection based estimators

In the application from Figs. 5-6, $F(s)$ is selected as a 2^{nd}-order LPF with $b_2 = b_1 = 0$, and $b_0 = a_0$. For a cut-off frequency $\omega_0 = 200$ rad/s and a damping factor $\xi = 0.7$, the BPF parameters are: $a_0 = 200^2$, $a_1 = 280$, $\omega_c = 2\pi\,400$ rad/s.

Finally, Fig. 8 presents the BPF frequency distribution and bandwidths for all three estimators based on signal injection. The required BPF bandwidths for the estimators are: $4\omega_{rmax}$ for STe-Cr, FDe-Sr estimators; and $2\omega_{rmax}$ for both BPFs of MPe-Rr^ estimator, where ω_{rmax} is the maxim rotor speed.

D. Initial Rotor Position Identification

The initial rotor position identification of IPMSM at standstill is mandatory in order to avoid temporary reverse rotation at startup or starting failure.

A simple approach aligns the rotor to a known initial position at startup using a specific inverter pattern, but the rotor moves, moreover in unpredictable direction.

If the initial rotor position is in range of $[-\pi/2, \pi/2]$ then its identification is successfully done at standstill using any of the three-presented estimators based on signal injection. An uncertainty of π radians appears for full angle range.

For rotor position identification in full range at standstill, the key is to decide the magnet polarity by other methods based on saturation saliency. One-approach employs 2^{nd} hf carrier-current harmonics with very low amplitudes using first order d-axis inductance saturation-model [4-5]. Other approaches, based on pulse pattern signal injection, estimate the minimum inductance location by evaluate di_s/dt as the INFORM (INdirect Flux detection by On-line Reactance Measurement) method [10].

IV. COMPARATIVE SIMULATION RESULTS

The test bench to compare the three estimators consists in a signal generator to simulate the stator-current vector containing carrier-harmonics $\underline{i}_{sc}$ (3) of IPMSM excited by hf signal injection (2). The test signal parameters are:
$I_s = 3$A, $I_{cp1} = 13$A, $I_{cn1} = 5$A, $I_{cp2} = I_{cn2} = 0.2$A,
$\Phi_{p2} = \Phi_{n2} = \pi/4$, $\Phi_s = 0$ and $\omega_c = 2\pi\,400$ rad/s.

The rotor position test-signal is chosen with constant speed $\theta_r = \omega_r t + \theta_{r0}$, where θ_{r0} is the initial rotor position. This ramp test signal checks the estimators tracking behavior. For $\omega_r = 0$, the estimators will identify the rotor position at standstill.

The parameters of the estimators (E1, E2, E3) are:

E1) STe-Cr (Fig. 3): 1^{st}-order LPF with T_f = 1ms; PLL compensator with $k_p = 100$, $k_i = 5000$.

E2) MPe-Rr^ (Fig.5): 2^{nd}-order BPF (Fig.7) with $a_0 = 200^2$, $a_1 = 280$; PLL compensator with $k_p = 50$, $k_i = 1000$

E3) FDe-Sr (Fig. 6): 2^{nd}-order BPF (Fig. 7) with $a_0 = 200^2$, $a_1 = 280$; PLL compensator with $k_p = 100$, $k_i = 5000$.

The simulations use Matlab-Simulink package with 4^{th}-order Runge-Kutta integration method. The sampling rate is $h = 100$ µs, typical for IGBT invertors.

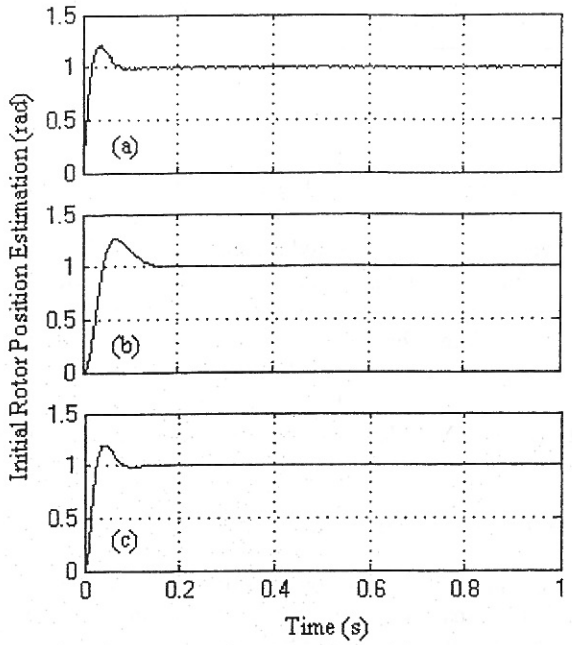

Fig. 9. Initial rotor position estimation for $\theta_{r0} = 1$ rad, $\omega_r = 0$ rad/s, using the estimators: (a) STe-Cr, (b) MPe-Rr^, (c) FDe-Sr

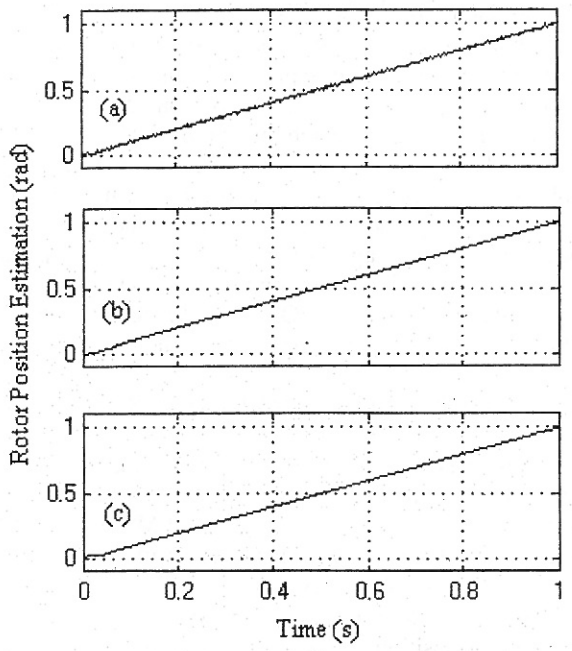

Fig. 10. Rotor position estimation for $\theta_{r0} = 0$ rad, $\omega_r = 1$ rad/s, using the estimators: (a) STe-Cr, (b) MPe-Rr^, (c) FDe-Sr

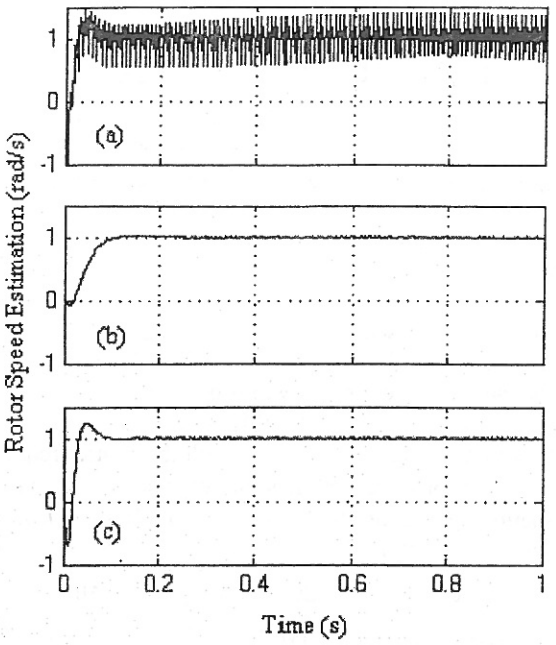

Fig. 11. Rotor speed estimation for $\theta_{r0} = 0$ rad, $\omega_r = 1$ rad/s, using the estimators: (a) STe-Cr, (b) MPe-Rr^, (c) FDe-Sr

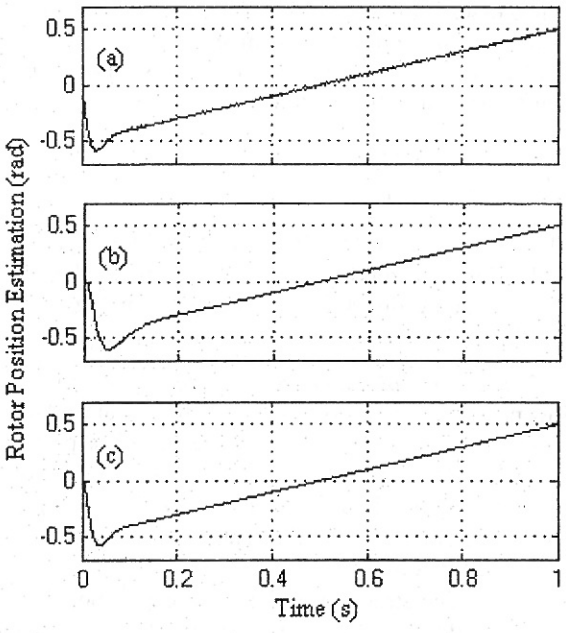

Fig. 12. Rotor position estimation for $\theta_{r0} = -0.5$ rad, $\omega_r = 1$ rad/s, starting from $\hat{\theta}_{r0} = 0$, using estimators: (a) STe-Cr, (b) MPe-Rr^, (c) FDe-Sr

The first test illustrates the identification of initial rotor position $\hat{\theta}_{r0}$ at standstill, for $\theta_{r0} = 1$ rad and $\omega_r = 0$ in (11). Fig. 9 shows initial rotor position estimations of E1, E2, E3 estimators respectively, with $\theta_{r0} = 1$ rad. The extensive simulations prove the correct estimations of initial rotor position if $\theta_{r0} \in (-\pi/2, \pi/2)$. An uncertainty of π radians appears for full angle range.

The second test illustrates the tracking behaviour of the estimators for a ramp signal (11) with very low speed $\omega_r = 1$ rad/s.

Fig. 10 shows rotor position estimations $\hat{\theta}_r$ and Fig. 11 shows rotor speed estimations $\hat{\omega}_r$ of E1, E2, E3 estimators respectively, with $\hat{\theta}_{r0} = 0$.

In Fig. 12 initial position is $\theta_{r0} = -0.5$ rad while the estimators start with $\hat{\theta}_{r0} = 0$. They shortly estimate the initial position in less then 100 ms, then tracks the linear rotor position.

Fig. 13 shows the negative carrier-current i_{cn1} extracted using vector filter in D-module in estimator E2 and E3.

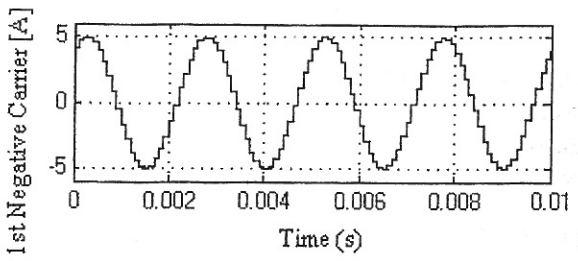

Fig.13. Negative carrier-current i_{cn1} extracted of vector filter in D-module

The simulation results demonstrate the effectiveness and the equivalence of the three estimators at low and zero speed. The new estimator seems to have more accuracy, high-dynamics and noise rejection.

V. CONCLUSIONS

Three integrated sensors (estimators) of rotor position and speed based on the rotating carrier-voltage vector injection and spatial saliency using stator carrier-current harmonics in different reference frames have been investigated for sensorless control of IPMSM drives.

The important features are the following:

- An efficient vector band-pass filter (BPF) of n^{th}-order two-input/output filter in D-module is used, which processes the negative or positive sequence based on frequency polarity. It has a high signal-to-noise ratio (SNR), and rejects the effect of dc-offset and drift from the stator current acquisition chains.
- The PLL tracking observer extracts the rotor position and speed from the phase of the selected carrier-current harmonic, i.e. usually the negative sequence in different references. The rotor estimation is not sensitive to the harmonic amplitude, which depends on inductances through saturation phenomena. Thus the estimations are very robust to all motor parameters.
- A high-bandwidth dynamic estimation with zero-phase lag can be obtained by using in PLL of an extended Luenberger observer with estimated torque as input.
- The new integrated sensor, based on a single vector BPF using 2^{nd}-order two-input/output filter in D-module in stator reference, cascaded by a PLL tracking observer, has the simplest realization preserving the good results.
- The initial rotor position is correctly identified at standstill by any of the three-presented estimators in the $[-\pi/2, \pi/2]$ range. For full angle range, an uncertainty of π radians appears, and the magnet polarity detection should be employed using other methods.
- The extensive simulation results prove the effectiveness and the equivalence of these integrated sensors. They present robustness and very good estimation performances at low speed including zero speed.
- The new estimator seems to have more accuracy, high-dynamics and noise rejection.

VI. REFERENCES

[1] I. Boldea and S. A. Nasar, *Electric Drives*, CRC Press, Boca-Raton, Fl., USA, 1999.

[2] J. Holtz, "Sensorless control of induction machoines – with or without signal injection ?," in *Proc. 9th Int. Conf. on Optimization of Electrical and Electronic Equipments OPTIM 2004*, Brasov, Romania, May 2004, Keynote, XVII-XL.

[3] M. W. Degner and R. D. Lorenz, "Using multiple saliencies for the estimation of flux, position, and velocity in AC machines," *IEEE Trans. Industry Applications*, vol. 34, no. 54, Sept./Oct. 1998, pp. 1097-1104.

[4] H. Kim, K.-K. Huh, M. Harke, J. Wai, R. D. Lorenz and T. M. Jahns, "Initial rotor position estimation for an integrated starter alternator IPM synchronous machine," in *Proc. 10th European Power Electronics and Applications Conf. EPE 2003*, Toulouse, France, Sept. 2003, CDROM: 0729.pdf, pp. 1-9.

[5] Y. Jeong, R.D. Lorenz, T.M. Jahns and S. Sul, "Initial rotor position estimation of an interior permanent magnet synchronous machine using carrier-frequency injection methods," in *Proc. IEEE Int. Electric Machines and Drives Conf. IEEE-IEMDC'03*, Madison, WI, USA, June 2003, vol.2, pp. 1218-1223.

[6] M. Linke, R. Kennel and J. Holtz, "Sensorless speed and position control of synchronous machines using alternating carrier injection," in *Proc. IEEE Int. Electric Machines and Drives Conf. IEEE-IEMDC'03* Madison, WI, USA, June 2003, vol.2, pp. 1211-1217.

[7] C. Silva, G. M. Asher, M. Summer and K.L. Bradley, "Sensorless rotor position control in surface mounted PM machine using hf voltage injection," in *Proc. 10th Int. Conf. of Power Electronics and Motion Control EPE-PEMC 2002*, Dubrovnik & Cavtat, Croatia, Sept. 2002, CDROM: SSAC-03.pdf, pp. 1-10.

[8] S. Shinnaka, "New "Mirror-phase vector control" for sensorless drive of IPM synchronous motor," in *Proc. IEEE Int. Electric Machines and Drives Conf. IEEE-IEMDC'03*, Madison, WI, USA, June 2003, vol. 3, pp. 1875-1881.

[9] S. Shinnaka, "A new characteristics-variable two-input/output filter in D-module–Designs, realizations, and equivalences" *IEEE Trans Industry Applications*, vol. 38, no. 5, Sept./Oct. 2002, pp. 1290-1296.

[10] M. Schroedl, E. Robeischl and T. Colle, "Sensorless INFORM-based position drives," in *Proc. 37th International Intelligent Motion Conf. PCIM 2000 Europe*, Nurnberg, Germany, June 2000, pp. 113-119.